Available online at www.sciencedirect.com
SCIENCE DIRECT
Journal of Power Sources 156 (2006) 489–496
JOURNAL OF POWER SOURCES
www.elsevier.com/locate/jpowsour

Simulation of a low temperature water gas shift reactor using the heterogeneous model/application to a pem fuel cell

Pablo Giunta, Norma Amadeo, Miguel Laborde *

Chemical Engineering Department, School of Engineering, Universidad de Buenos Aires, Pabellón de Industrias, Ciudad Universitaria, 1428 Buenos Aires, Argentina

Received 8 March 2005; accepted 19 April 2005
Available online 15 July 2005

Abstract

In the last few years, a renewed interest in the water gas shift (WGS) reaction at low temperature has arisen due to its application to fuel cells.

In this work, a simulation of a fixed bed reactor for this reaction, which forms part of a hydrogen production–purification train for a 10 kW PEM fuel cell using ethanol as the raw material, was carried out. A commercial $Cu/Zn/Ba/Al_2O_3$ catalyst was employed and a one-dimensional heterogeneous model was applied for the simulation. The catalyst deactivation due to thermal factors (sintering) was taken into account in the model. Isothermal and adiabatic regimes were analyzed as well.

Results of the simulation indicate that the pellet can be considered isothermal but temperature gradients in the film cannot be disregarded. On the other hand, concentration gradients in the film can be ignored but CO profiles are established inside the pellet. Adiabatic operation can be recommended because of its simplicity of operation and construction. The reactor volume is strongly sensitive to the CO outlet concentration at CO levels lower than 6000 ppm. For a 10 kW PEM fuel cell, using adequate pellet size and taking into account the catalyst deactivation, a reactor volume of 0.64 l would be enough to obtain an outlet CO concentration of about 7160 ppm. This concentration value can be handled by the next purification stage, COPROX.

Keywords: WGS reactor design; Hydrogen production; Fuel cell

1. Introduction

The clean and non-contaminating characteristics of H_2 as a fuel will depend on the process, the raw material and the source of energy employed for its production. If it is obtained from fossil hydrocarbons, carbon dioxide is released to the atmosphere, regardless of the technology used; if biomass is used instead of hydrocarbons, carbon dioxide is also released, but in this case the plant consumes the carbon dioxide produced during its growth. Thus, the qualification of "clean" fuel is only true if the raw material is biomass. Ethanol is a renewable, non-toxic and easy to manipulate source, and has therefore excellent chances to replace fossil fuels [1].

The new application of H_2 as a raw material for fuel cells for mobile power sources (PEM fuel cells) requires that the anode inlet gas have a CO concentration lower than 10–20 ppm. Otherwise, the anode is poisoned and the cell efficiency abruptly drops.

Hence, if the H_2 is produced from hydrocarbons or alcohol reforming, purification is required in order to reduce the CO levels to cell requirements. So far, the most technologically feasible purification train consists of a water gas shift converter (WGS) and a latter step of remaining CO elimination. According to Zalc and Löffler [2], the WGS reactor is expected to have the largest volume, and is limited by the catalyst intrinsic activity.

The reaction

$$CO + H_2O = CO_2 + H_2,$$

$$\Delta H^0_{298} = -4.11 \times 10^{11}\ \text{erg mol}^{-1} (-41.1\ \text{kJ mol}^{-1})$$

* Corresponding author. Tel.: +54 11 45763240; fax: +54 11 45763240.
E-mail address: miguel@di.fcen.uba.ar (M. Laborde).

0378-7753/$ – see front matter © 2005 Elsevier B.V. All rights reserved.
doi:10.1016/j.jpowsour.2005.04.036

Nomenclature

a	activity (–)
a_∞	residual activity (–)
A	reactor cross-section area (cm^2)
Bi_m	mass Biot number (–)
C	concentration ($mol\,cm^{-3}\,s^{-1}$)
Cp_m	heat capacity of gas mixture ($erg\,mol^{-1}\,K^{-1}$)
$\mathcal{D}_e$	reaction diameter (cm)
$\mathcal{D}_{ef}$	effective diffusion coefficient ($cm^2\,s^{-1}$)
F	mole flow ($mol\,s^{-1}$)
G	mass flux ($g\,cm^{-2}\,s^{-1}$)
ΔH	reaction molar enthalpy ($erg\,mol^{-1}$)
k	reaction rate constant ($mol\,g^{-1}\,s^{-1}\,atm^{-1.225}$)
k_d	deactivation rate constant (s^{-1})
K_{eq}	equilibrium constant (–)
k_m	mass transfer coefficient ($cm\,s^{-1}$)
L	reactor length (cm)
n	deactivation order (–)
P	pressure (atm)
Pe_p	Peclet number (–)
ΔP	pressure drop (atm)
R_G	gas constant ($cm^3\,atm\,mol^{-1}\,K^{-1}$)
R_p	pellet radius (cm)
R_V	reaction rate ($mol\,cm^{-3}\,s^{-1}$)
t	time (s)
T	temperature (K)
u_z	Gas velocity ($cm\,s^{-1}$)
v	trial value (–)
V	reactor volume (cm^3)
x	CO conversion (–)
y	mole fraction (–)
z	dimensionless axial variable (–)
Z	axial variable (cm)

Greek letters

α	stoichiometric coefficient (–)
β	equilibrium approach factor (–)
χ	auxiliary variable N°1 (–)
ε	error function (–)
ε_b	bed porosity (–)
Φ	Thiele modulus (–)
η	effectiveness factor (–)
κ	thermal conductivity coefficient ($erg\,cm^{-1}\,K^{-1}$)
μ	gas viscosity ($g\,cm^{-1}\,s^{-1}$)
ν	reaction order (–)
θ	dimensionless temperature
ρ	gas density ($g\,cm^{-3}$)
τ	dimensionless reactor volume (–)
ω	dimensionless radial variable (pellet) (–)
ξ	dimensionless concentration (–)
ψ	auxiliary variable N°2 (–)
Ω	radial variable (pellet) (cm)

Subscripts and superscripts

g	Value at bulk gas
i	Species i
k	kth iteration
s	Value at surface
T	Total
0	Inlet/reference conditions

has been employed for 40 years in the industrial process for H_2 production from liquid and gaseous hydrocarbons. The role of the WGS reaction is to increase the H_2 yield and decrease the CO concentration, which is a poison for some catalysts used downstream like in ammonia synthesis or oil dehydrogenation. The WGS reaction is traditionally carried out in two fixed bed adiabatic reactors, connected in series with a cooler between them. The first reactor operates at temperatures ranging from 300 to 500 °C and employs a Fe/Cr catalyst. The second reactor operates at lower temperatures (180–300 °C) in order to displace the equilibrium, since the WGS reaction is exothermic, and uses a Cu/Zn/Al catalyst. Several studies that intended to elucidate the kinetics and reaction mechanism [3–21], as well as the deactivation by poisoning [22], have been carried out, Chocrón et al. [23] have analyzed the mass transfer in a Cu/Zn/Al catalyst subject to deactivation and González-Velasco et al. [24], considering catalyst deactivation, have proposed optimal practices for an industrial reactor operation.

Recently a renewed interest in the study of this reaction has arisen due to its application to fuel cells. Several works on different catalysts more active than the traditional one, which can be used for H_2 production for a fuel cell, have been published. Some authors propose the doping of Cu/Zn/Al based catalysts [25]. Some of them suggest the use of the commercial Cu/Zn/Al catalyst by adding O_2 to the feed to oxidize the CO [26]. Other authors have used noble metals [27,28]. Finally, the majority reject traditional catalysts and propose the use of supported noble metals, ceria being the most commonly used support [29–34]. Zalc et al. [33], after working with a 1.5% Pt/CeO_2 catalyst and making an accurate analysis of works in which platinum and ceria are used, conclude that efforts should be focused on finding commercially viable catalysts, using lower cost metals, than those traditionally used, which is a good starting point.

In agreement with Zalc's arguments [2,33], a simulation of a fixed bed reactor for the WGS reaction, which forms part of a purification train for a 10 kW PEM fuel cell, was carried out in this work. A commercial $Cu/Zn/Al_2O_3$ catalyst doped with Ba was used because it showed a higher activity than the traditional one. The one-dimensional heterogeneous model was applied in this simulation, and a parametric sensitivity analysis was carried out for some of the process variables,

with the purpose of finding criteria to minimize the reactor volume.

2. Methodology

2.1. Description of the model

The heterogeneous one-dimensional model used in this work takes into account the existence of concentration and temperature gradients inside the catalytic pellet as well as in the external film. Regarding the fluid dynamics, the plug flow model can be applicable if in Eq. (1) is fulfilled [35]

$$\frac{L}{R_p} > \frac{40\,\nu_{CO}}{Pe_p} \ln\left(\frac{1}{1-x}\right). \tag{1}$$

A power law intrinsic kinetics with a term that takes into account the reversibility of this reaction is used [18]

$$R_V = k\, P_{CO}^{\nu_{CO}} P_W^{\nu_W} P_{CO_2}^{-\nu_{CO_2}} P_{H_2}^{-\nu_{H_2}} (1-\beta) \tag{2}$$

where

$$\beta = \frac{P_{CO_2}}{P_{CO}} \frac{P_{H_2}}{P_{H_2O}} \frac{1}{K_{eq}} \tag{3}$$

The catalyst deactivation was assumed to be only due to thermal effects (sintering)

$$\frac{da}{dt} = -k_d (a - a_\infty)^n \tag{4}$$

where a_∞ is the residual activity.The activity is defined as

$$a(t) = \frac{R_V(t)}{R_V(0)} \tag{5}$$

ν_i, k, n, a_∞ and k_d values in Eqs. (2) and (5) were experimentally obtained using a fixed bed lab scale reactor. These values are not reported because of confidentiality.

The system is divided into two subsystems: the pellet and the reactor (or bulk). The pellet must be solved first. This subsystem is a second order non-linear boundary value problem, whereas the reactor subsystem is a first order.

2.2. Pellet

The Thiele modulus is [36]

$$\Phi = \frac{R_p}{3}\sqrt{\frac{-\alpha R_V^s}{\mathcal{D}_{ef} C^g}} \tag{6}$$

In this definition the surface and bulk concentration are assumed to be equal since the difference between them was negligible (see Fig. 3).

The mass balance for reference species CO is

$$\frac{d^2C}{d\Omega^2} = \begin{cases} \dfrac{-\alpha R_V}{\mathcal{D}_{ef}} - \dfrac{2}{\Omega}\dfrac{dC}{d\Omega} & \Omega > 0 \\ \dfrac{-\alpha R_V}{3\mathcal{D}_{ef}} & \Omega = 0 \end{cases} \tag{7}$$

In Eq. (7) the origin of coordinates corresponds to the centre of the pellet. It should be noted that the function including the term with the first derivative has a singularity at $\Omega = 0$, so it cannot be used at this position. Instead, the limit of the expression must be used.

Since the pellet can be considered isothermal (as it will be proven later), the transport properties are assumed to be constant. Thus, it is possible to express the species i and T as linear functions of the reference species.

$$C_i - C_i^s = \frac{\alpha_i}{\alpha}\frac{\mathcal{D}_{ef}}{\mathcal{D}_{ef,i}}(C - C^s) \tag{8}$$

$$T - T^s = \frac{\mathcal{D}_{ef}(-\Delta H_r)}{\alpha \kappa_{ef}}(C - C^s) \tag{9}$$

where the reference species has no subscript.The boundary conditions are

$$\left.\frac{dC}{d\Omega}\right|_0 = 0 \tag{10}$$

$$\left.\frac{dC}{d\Omega}\right|^s = \frac{k_m}{\mathcal{D}_{ef}}(C^g - C^s) \tag{11}$$

Defining the mass Biot number (Eq. (12)), Eqs. (10) and (11) the dimensionless boundary conditions are given by Eqs. (13) and (14)

$$Bi_m = \frac{k_m R_p}{\mathcal{D}_{ef}} \tag{12}$$

$$\left.\frac{d\xi}{d\omega}\right|_0 = 0 \tag{13}$$

$$\left.\frac{d\xi}{d\omega}\right|_1 = Bi_m(1 - \xi|_1) \tag{14}$$

Finally, the effectiveness factor is

$$\eta = \frac{\bar{R}_V}{R_V^s} = \frac{3}{R_V^s\, 4\pi R_p^3}\int_0^{R_p} R_V\, 4\pi\Omega^2\, d\Omega \tag{15}$$

Eq. (15) can be rearranged introducing Eqs. (6), (12) and (14) in order to obtain a more convenient expression of η in terms of Φ, Bi_m and the surface concentration of the reference species

$$\eta = \frac{1}{3\Phi^2} Bi_m(1 - \xi|_1) \tag{16}$$

2.3. Reactor

Mass, energy and momentum balances are

$$\frac{dC}{dz} = \frac{\alpha\eta R_V^s(1-\varepsilon_b)}{u_z} + \frac{C}{C_T}\left(\frac{1}{R_G T}\frac{dP}{dz} - \frac{P}{R_G T^2}\frac{dT}{dz}\right) \tag{17}$$

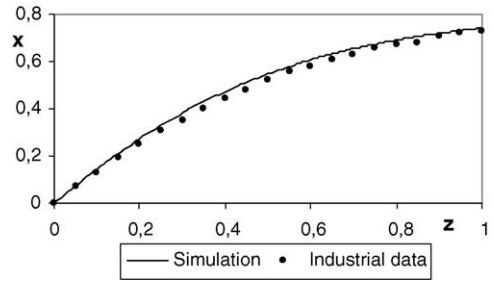

Fig. 1. Simulation results and industrial data. CO conversion (x) vs. dimensionless reactor length (z).

$$\frac{dT}{dz} = \frac{(-\Delta H_r)\eta R_V^s(1-\varepsilon_b)}{Cp_m} A \quad (18)$$

$$\frac{dP}{dz} = 9869 \times 10^{-7} \times \left(175\frac{G^2(1-\varepsilon_b)}{2\varepsilon_b^3 \rho R_p} + 150\frac{G\mu(1-\varepsilon_b)}{4\varepsilon_b^3 \rho R_p^2}\right)\frac{1}{A} \quad (19)$$

3. Algorithms

Simple first order differential equations are solved by the fourth order Runge–Kutta method.

However, non-linear boundary value problems cannot be solved as simply as first order initial value problems. The inverse shooting method was used to accomplish this task [37,38] (see Appendix A).

When this method is applied, the order of integration is reversed; therefore, the origin of coordinates corresponds to the pellet surface, while the end is the centre of the pellet.

3.1. Validation of the model

The model was compared with experimental data from two industrial reactors reported by Elnashaie and Elshishini [39]. The kinetics was taken from Rase [40]. Results are shown in Fig. 1. As it can be seen, the agreement is quite satisfactory.

4. Results and discussion

The analysis was carried out considering that the gas mixture entering the reactor has a composition similar to that of an ethanol steam reformer outlet, namely, CO, CO_2, H_2 and CH_4. Also, the study was carried out considering that the H_2 produced must feed a 10 kW PEM fuel cell.

Unless otherwise informed, the analysis was performed at time 0 – without deactivation – and considering adiabatic operation.

Operating conditions are listed in Table 1.

A comment should be made about the pressure value. As the PEM fuel cell feed pressure is near 4.5 atm [44], it seems to be more convenient to increase the pressure before the WGS stage rather than before the fuel cell. Fig. 2 indicates the effect of pressure on the WGS performance. It can be seen that the CO conversion is favoured when pressure increases.

Table 1
Basic operating conditions

T (K)	473
P (atm)	5
F (mol s^{-1})	0.32
R_p (cm)	0.285
V (cm^3)	3927
y_{CO}	0.06
y_W	0.40
y_{CO_2}	0.12
y_{H_2}	0.40
y_{CH_4}	0.02

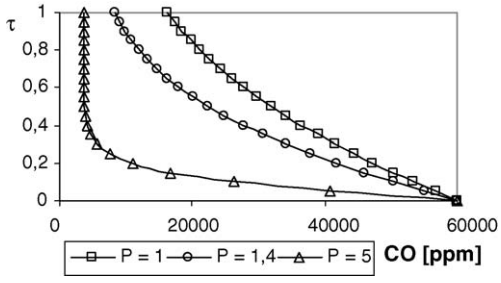

Fig. 2. Dimensionless reactor volume (τ) vs. CO outlet concentration [ppm] at different P [atm].

4.1. Effect of pellet radius

Fig. 3 shows that CO profiles depart from 1 regardless of the pellet radius, indicating that the bulk and surface compositions can be considered equal. In addition, these profiles become steeper as the particle size increases. The mass transfer resistance in the film is only detected when the gas flow in the reactor falls to approximately a 5% of the value given in Table 1 [41].

Temperature profiles are flat throughout the pellet radius (Fig. 4), regardless of its size. Nevertheless, each profile departs from a different value, clearly showing the effect of

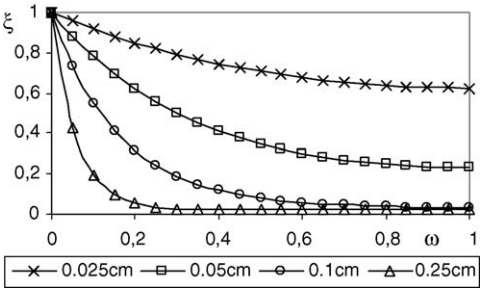

Fig. 3. Dimensionless CO concentration (ξ) vs. dimensionless pellet radius (ω) for different R_p.

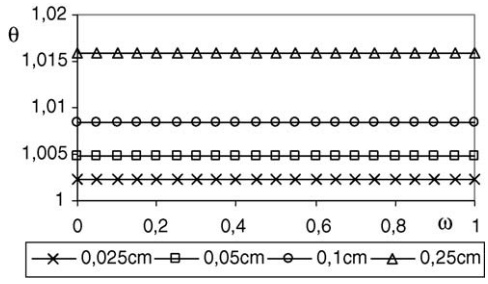

Fig. 4. Dimensionless temperature (θ) vs. dimensionless pellet radius (ω) for different R_p.

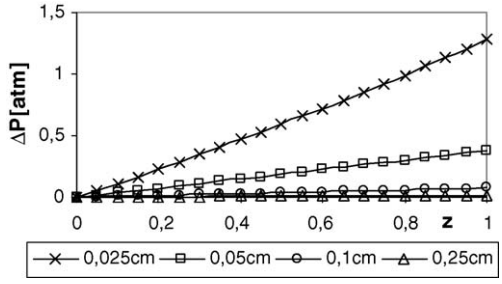

Fig. 5. Pressure drop (ΔP) vs. dimensionless reactor length (z) for different R_p.

the film. When the gas flow is decreased, this effect is more pronounced on temperature profiles than on CO profiles [41].

The effect of the pellet size on the pressure drop and CO conversion is shown in Figs. 5 and 6, respectively. It can be seen that ΔP increases and the CO conversion decreases when the pellet radius decreases. Thus, the size of the pellet is a trade-off between pressure drop and conversion.

4.2. Effect of the inlet temperature

Fig. 7 indicates the reactor volume required to reach a given CO exit concentration. As can be seen, on one hand, if the CO exit concentration is not critical, high inlet temperatures are more convenient due to the thermal effects on the kinetics. On the other hand, for higher CO removal, low inlet temperatures are more suitable due to the thermal effects on the equilibrium. The strong dependence of the reactor volume on CO concentration values near equilibrium should be outlined.

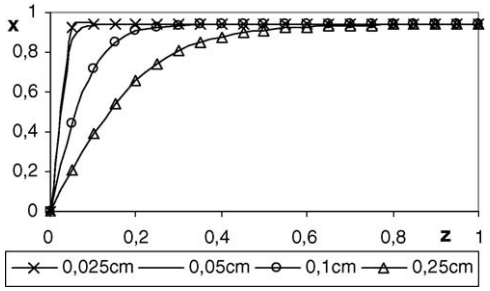

Fig. 6. CO conversion (x) vs. dimensionless reactor length (z) for different R_p.

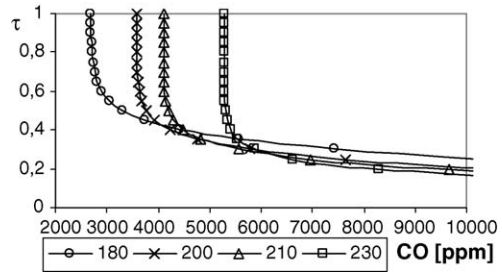

Fig. 7. Dimensionless reactor volume (τ) required for a given exit CO concentration at different T^0.

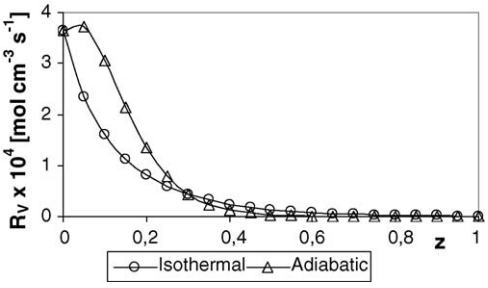

Fig. 8. Reaction rate (R_v) vs. dimensionless reactor length (z) for isothermal and adiabatic operation.

4.3. Adiabatic versus isothermal

The reaction rate and conversion profiles along the reactor for these thermal regimes are shown in Figs. 8 and 9, respectively. The reaction rate for the adiabatic reactor shows a maximum because of the opposite effects of concentration and temperature, whereas in the isothermal case, the reaction rate always decreases (Fig. 8). In the first part of the reactor, where kinetic effects are preponderant, the reaction rate for the adiabatic case is larger than that in the isothermal case. Thus, profiles develop more rapidly. However, as the reaction is exothermic, higher temperatures obtained in the adiabatic reactor yield a lower conversion (Fig. 9).

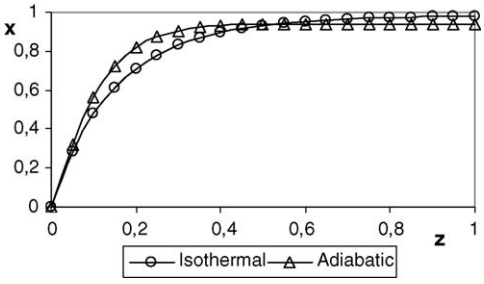

Fig. 9. CO conversion (x) vs. dimensionless reactor length (z) for isothermal and adiabatic operation.

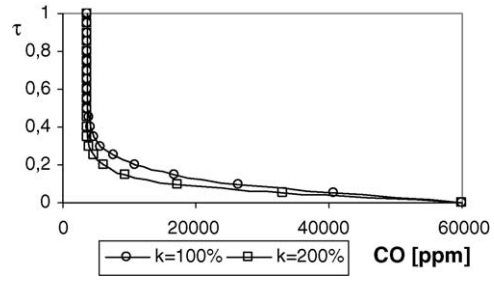

Fig. 10. Dimensionless reactor volume (τ) required for a given outlet CO composition [ppm] for two different catalyst activities.

4.4. Effect of activity

Fig. 10 shows the reactor volume required to reach a given exit concentration using the actual catalyst ($k = 100\%$) and a catalyst twice as active as the original one ($k = 200\%$).

It can be seen that the reactor volume is not as sensitive to the catalyst activity as it would be expected. When the activity was increased by a 100%, the average conversion increased only a 35% at the inlet, where the reaction rate is the highest. This is due to the fast approach to equilibrium inside the pellet, which causes the effectiveness factor value to decrease. Thus, the pellet acts as a "buffer".

4.5. Effect of reactor diameter

For a given pellet size, pressure is the most strongly affected variable by the reactor diameter. It can be observed from Fig. 11 that, for diameters larger than 7.5 cm, the reactor can be considered isobaric. The pressure drop is relevant for diameters smaller than 3.5 cm. It can be concluded that there is a minimum diameter given by the pressure drop and a maximum diameter given by the plug flow condition (in Eq. (1)).

4.6. Effect of the operation time

In Fig. 12, the reactor volume required to reach a given CO exit concentration for different operation times is shown. Due to the deactivation, for a given CO concentration the reactor

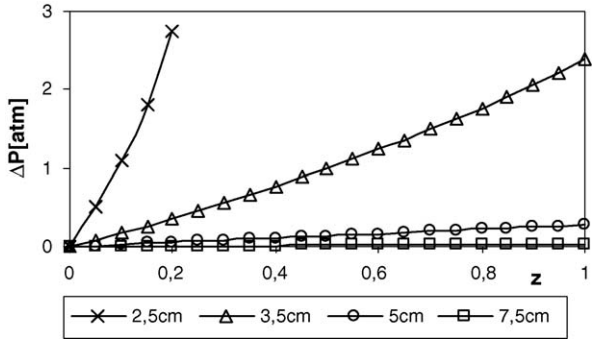

Fig. 11. Pressure drop (ΔP) vs. dimensionless reactor length (z) for different D_R.

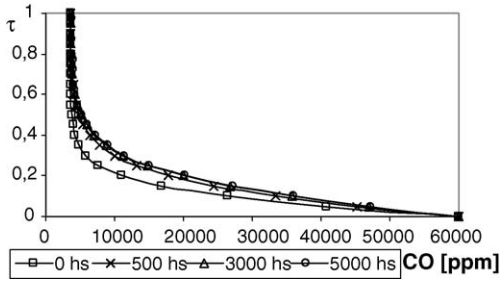

Fig. 12. Dimensionless reactor volume (τ) required for a given outlet CO composition [ppm] for different operation times.

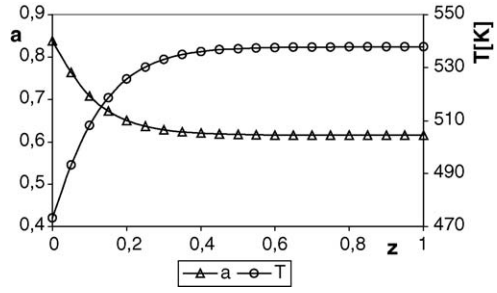

Fig. 13. Activity (a) and temperature (T) vs. dimensionless reactor length (z) at a given operation time.

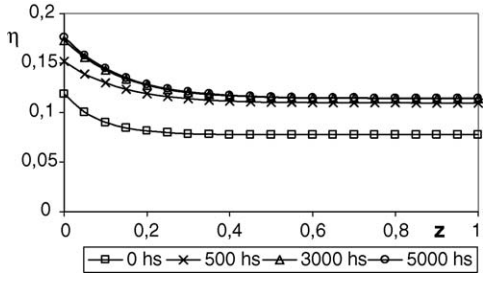

Fig. 14. Effectiveness factor (η) vs. dimensionless reactor length (z) at different operation times.

volume increases with the operation time. A convergence of curves is observed for $t \to \infty$ because of the existence of a non-zero residual activity (see Fig. 12). The effect of the deactivation on the reactor performance is similar to that observed on Fig. 10, since in both analyses there is a change in the activity.

Since the activity only depends on the temperature (besides time), a temperature profile produces an activity profile along the reactor. This is shown in Fig. 13.

As the activity decreases, the effectiveness factor increases (Fig. 14) because the pellet is more uniformly used. Once more, the effectiveness factor acts as a "buffer".

5. Conclusions

In this work, the simulation of the WGS reactor was performed, applying the one-dimensional heterogeneous model. In the studied cases, the isothermicity of the pellet and the

existence of temperature gradients in the film were demonstrated (Fig. 4). This gradient increases with increasing pellet size and decreasing gas flow. As regards mass transfer, concentration profiles are developed inside the pellet, and become steeper with increasing pellet size. On the other hand, film resistance can be neglected (Fig. 3).

Although under certain conditions isothermal operation would allow higher conversions, these improvements do not seem significant; thus, adiabatic operation is chosen due to its simplicity.

The COPROX reactor, which should be downstream with respect to the WGS stage, can handle an inlet gas mixture with a CO concentration between 2000 and 20000 ppm [42,43]. According to Fig. 7, the required reactor volume is strongly sensitive to the CO outlet concentration for CO levels lower than 6000 ppm (depending on the inlet temperature). For a CO concentration of 3580 ppm, operating adiabatically with $T^0 = 200\,^{\circ}\mathrm{C}$, $P = 5$ atm, $R_p = 0.285$ cm (commercial size), the reactor volume for a 10 kW PEM fuel cell should be of approximately 4 l (Table 1). A reactor diameter of 7.5 cm and a length of around 90 cm satisfy the plug flow hypothesis and produce a negligible ΔP (see Figs. 5 and 11). These values were obtained at $t = 0$, namely $a = 1$. If this analysis is repeated for a CO concentration of 7160 ppm – twice as higher as the original value – the reactor volume is reduced by 74%, that is to say, to around 1 l, with a reactor diameter of 4.8 cm and a length of 57.6 cm, dimensions that fulfil in Eq. (1).

The reactor size can also be reduced by working with a smaller pellet size (due to the rise of the effectiveness factor and residence time), always checking the pressure drop. If the pellet size is 0.1 cm the pressure drop is still very low (see Fig. 5). In this case, for a CO outlet concentration of 7160 ppm, the reactor volume is reduced by 90%, i.e. 0.4 l. Taking into account the catalyst deactivation, the reactor volume can be reduced by 84%, namely to 0.64 l.

As a car requires a 60 kW PEM fuel cell, an alternative would be to place six reactors of the same size in parallel. A single reactor with a volume the sum of six reactors does not seem to be an appropriate alternative, as depicted in Figs. 6 and 12.

So, performing an overall analysis, and taking into account the operation variables and reactor and pellet geometry, it is possible to achieve reasonable volumes to the WGS reactor. These volumes will also depend on the inlet conditions that a COPROX reactor can handle – which are in fact the WGS outlets – considering that, the lower the WGS conversion is, the higher the amount of oxidized hydrogen in the COPROX stage will be.

Acknowledgments

The authors acknowledge the financial support of University of Buenos Aires, ANPCyT, CONICET, CYTED and Química Abengoa.

Appendix A

A.1. The shooting method

This method consists of two stages: integration along the spatial position and correction of the trial value. The trial value is the dimensionless surface concentration of the reference species.

Once the reference species profile is solved inside the pellet, the effectiveness factor can be calculated by means of Eq. (16) and used to compute Eqs. (17) and (18). These two equations, together with Eq. (19), are used to calculate bulk conditions throughout the reactor.

A.2. Integration

Making Eq. (7) dimensionless and introducing the change of variable $\omega = \frac{R_p - \Omega}{R_p}$, Eq. (20) can be derived

$$\frac{\mathrm{d}^2\xi}{\mathrm{d}\omega^2} = \begin{cases} \dfrac{-\alpha R_p^2 R_V}{D_{ef} C^g} + \dfrac{2}{1-\omega}\dfrac{\mathrm{d}\xi}{\mathrm{d}\omega} & \Omega > 0 \\ \dfrac{-\alpha R_p^2 R_V}{3 D_{ef} C^g} & \Omega = 0 \end{cases} \tag{20}$$

A.3. Correction of trial value

With the trial value v, the boundary condition at the centre of the pellet should be verified. This condition is expressed as an error that must be driven to zero. The error function defined in this way is a function of the trial value

$$\varepsilon(v) = \frac{\partial \xi}{\partial \omega}(1, v). \tag{21}$$

The mathematical "trick" consists in considering v as another independent variable (besides the position). Nevertheless, the error function so defined is only a function of v because the concentration derivative is always evaluated at $\omega = 1$. ε is equal to zero when the first derivative of the concentration at the centre is zero.

From other point of view, it can be said that $\varepsilon(v) = 0$ when v is the root of the function. Therefore, the situation is treated as a root finding problem. The Newton–Raphson method is implemented to achieve this goal

$$v^{k+1} = v^k - \frac{\varepsilon(v^k)}{\frac{\mathrm{d}\varepsilon}{\mathrm{d}v}(v^k)} \tag{22}$$

However, the denominator in Eq. (22) has not been defined yet. Two new variables are introduced

$$\chi = \frac{\partial \xi}{\partial v} \tag{23}$$

$$\psi = \frac{\partial \chi}{\partial \omega} \tag{24}$$

Combining Eqs. (21), (23) and (24), it can be seen that

$$\psi(1, v) = \frac{d\varepsilon}{dv}(v) \tag{25}$$

The differential equation that allows $\psi(1,v)$ to be calculated is obtained by derivating Eq. (20) with respect to v

$$\frac{d^2\chi}{d\omega^2} = \begin{cases} \dfrac{-\alpha R_p^2}{\mathcal{D}_{ef} C^g} \dfrac{\partial R_V}{\partial \xi} \chi + \dfrac{2}{1-\omega}\psi & \Omega > 0 \\ \dfrac{-\alpha R_p^2}{3\mathcal{D}_{ef} C^g} \dfrac{\partial R_V}{\partial \xi} & \Omega = 0 \end{cases} \tag{26}$$

This differential equation is solved together with Eq. (20). The value of ψ at $\omega = 1$ is used to compute Eqs. (21) and (22) and update the trial value.

References

[1] F. Mariño, PhD Thesis, University of Buenos Aires, 2001.
[2] J.M. Zalc, D.G. Löffler, J. Power Sources 111 (2002) 58–64.
[3] G.G. Shchibrya, Kinet. Katal. 6 (1965) 1115.
[4] F. Goodridge, H. Quazi, Trans. Inst. Chem. Eng. 45 (1967) 274.
[5] H. Bohlboro, M. Jorgensen, Chem. Eng. World 5 (1970) 46.
[6] G. Leherte, R. Derie, P.H. Duvigneaud, Preparation of Catalysts, Elsevier Science Publication, Amsterdam, 1976.
[7] T. Semenova, B. Lyudkovskaya, M. Markina, Ya. Volynkina, G. Cherkasov, V. Sharkina, N. Khitrova, G. Shpiro, Kinet. Katal. 18 (1977) 1014.
[8] T. van Herwijnen, W. de Jong, J. Catal. 63 (1980) 83.
[9] T. van Herwijnen, R. Guczalski, W. de Jong, J. Catal. 63 (1980) 94.
[10] E. Fiolitakis, H. Hofmann, J. Catal. 80 (1983) 328.
[11] G.C. Chinchen, P.J. Denny, D.G. Parker, G.D. Short, M.S. Spencer, K.C. Waugh, D.A. Whan, Proceedings of the ACS Symposium on Methanol and Synthetic Fuels, vol. 29, 1984, p. 178.
[12] E.G.M. Kuijpers, R.B. Tjepkema, W.J.J. van der Wal, Appl. Catal. 25 (1986) 139.
[13] C.T. Campbell, K.A. Daube, J. Catal. 104 (1987) 109.
[14] T. Salmi, R. Hakkarainen, Appl. Catal. 49 (1989) 285.
[15] E. Colbourn, R.A. Hadden, H.D. Vandervell, K.C. Waugh, G. Webb, J. Catal. 130 (1991).
[16] S.I. Fujita, M. Usui, N. Takezawa, J. Catal. 134 (1994) 220; S.I. Fujita, M. Usui, N. Takezawa, Chem. Lett. (1877).
[17] K.H. Ernst, C.T. Campbell, G. Moretti, J. Catal. 134 (1992) 66.
[18] N.E. Amadeo, E.G. Cerella, M.A. Laborde, F. Pennella, Latin Amer. Appl. Res. 25 (1995) 21.
[19] N.E. Amadeo, M.A. Laborde, Int. J. Hydrogen Ener. 20 (12) (1995) 949.
[20] C.V. Ovesen, B.S. Clausen, B.S. Hammershøi, G. Steffensen, T. Askgaard, I. Chorkendorff, J.K. Norskov, P.B. Rasmussen, P. Stoltze, P. Taylor, J. Catal. 158 (1996) 170.
[21] J.L. Ayastuy, M.A. Gutiérrez-Ortiz, J.A. González-Marcos, A. Aranzabal, J.R. González-Velasco, Ind. Eng. Chem. Res. 44 (2005) 41.
[22] M.L. Aparicio, M.A. Laborde, N.E. Amadeo, Inform. Tecnol. 7 (1996) 1.
[23] M. Chocrón, M.C. Raffo Calderón, N. Amadeo, M.A. Laborde, Chem. Eng. Sci. 51 (1996) 683.
[24] J.R. González-Velasco, M.A. Gutiérrez-Ortiz, J.A. González-Marcos, N. Amadeo, M.A. Laborde, M. Paz. Chem. Eng. Sci. 47 (1992) 1495.
[25] K. Klier, Ch. Young, J. Nunan, I EC Fundam. 25 (1986) 36–42.
[26] T. Utaka, K. Sekizawa, K. Eguchi, Appl. Catal. A: Gen. 194–195 (2000) 21–26.
[27] F. Boccuzzi, A. Chiorino, M. Manzoli, D. Andreeva, T. Tabakova, L. Ilieva, V. Idakiev, Catal. Today 75 (2002) 169–175.
[28] T. Tabakova, V. Idakiev, D. Andreeva, I. Mitov, Appl. Catal. A: Gen. 202 (2000) 91–97.
[29] T. Sido, Y. Iwasawa, J. Catal. 141 (1993) 71–81.
[30] T. Bunluesin, R. Gorte, G. Graham, Appl. Catal. B: Environ. 15 (1998) 107–114.
[31] Y. Li, Q. Fu, M.F. Stephanopoulos, Appl. Catal. B: Environ. 27 (2000) 179–191.
[32] S. Hilaire, X. Wang, T. Luo, R. Gorte, J. Wagner, Appl. Catal. A: Gen. 215 (2001) 271–278.
[33] J. Zalc, V. Sokolovskii, D. Loffler, J. Catal. 206 (2002) 169–171.
[34] N. Amadeo, M. Laborde, Trends Chem. Eng. 3 (1997) 159.
[35] J.A. Moulijn, A. Tarfaoui, F. Kapteijn, Catal. Today 11 (1991) 1–12.
[36] I.H. Farina, O.A. Ferretti, G.F. Barreto, Introducción al Diseño de Reactores Químicos. Ed. EUDEBA, Buenos Aires, 1986.
[37] M. Hlavacek, V. Kubicek, Numerical Solutions of Non-linear Boundary Value Problems with Applications, Prentice-Hall, 1983.
[38] D.H. Kim, J. Lee, Chem. Eng. Sci. 59 (2004) 2253–2263.
[39] S.S.E.H. Elnashaie, S.S. Elshishini, Modelling, Simulation and Optimization of Industrial Fixed Bed Catalytic Reactors, Gordon and Breach Science Publishers, 1993.
[40] H.F. Rase, Chemical Reactor Design for Process Plants, John Wiley and Sons, 1977.
[41] P.D. Giunta, Degree Thesis, University of Buenos Aires, 2004.
[42] F. Mariño, C. Descorme, D. Duprez, Appl. Catal. B: Environ. 54 (2004) 59.
[43] F. Mariño, C. Descorme, D. Duprez, Appl. Catal. B: Environ. 58 (2005) 175.
[44] C. Song, Catal. Today 77 (2002) 17–49.